



Article

Emission Factors of CO₂ and Airborne Pollutants and Toxicological Potency of Biofuels for Airplane Transport: A Preliminary Assessment

Maurizio Gualtieri ^{1,*†‡}, Massimo Berico ^{1,†}, Maria Giuseppa Grollino ^{2,*}, Giuseppe Cremona ¹, Teresa La Torretta ¹, Antonella Malaguti ¹, Ettore Petralia ¹, Milena Stracquadanio ¹, Massimo Santoro ², Barbara Benassi ², Antonio Piersanti ¹, Andrea Chiappa ³, Manuele Bernabei ³ and Gabriele Zanini ^{1,†}

¹ ENEA, Division of Models and Technologies for Risk Reduction, Via Martiri di Monte Sole 4, 40146 Bologna, Italy

² ENEA, Division of Health Protection Technologies, Via Anguillarese, 301, 00123 Rome, Italy

³ Italian Air Force, Aerospace Testing Division, Aerospace Materials and Technology Department, Aeroporto Militare de Bernardi 00071 Pratica di Mare, Pomezia, 00040 Rome, Italy

* Correspondence: maurizio.gualtieri@unimib.it (M.G.); maria.grollino@enea.it (M.G.G.)

† These authors contributed equally to this work.

‡ Present address: University of Milano-Bicocca, DISAT Piazza della Scienza 1.



Citation: Gualtieri, M.; Berico, M.; Grollino, M.G.; Cremona, G.; La Torretta, T.; Malaguti, A.; Petralia, E.; Stracquadanio, M.; Santoro, M.; Benassi, B.; et al. Emission Factors of CO₂ and Airborne Pollutants and Toxicological Potency of Biofuels for Airplane Transport: A Preliminary Assessment. *Toxics* **2022**, *10*, 617. <https://doi.org/10.3390/toxics10100617>

Academic Editor: João Fernando Pereira Gomes

Received: 20 September 2022

Accepted: 14 October 2022

Published: 18 October 2022

Publisher's Note: MDPI stays neutral with regard to jurisdictional claims in published maps and institutional affiliations.



Copyright: © 2022 by the authors. Licensee MDPI, Basel, Switzerland. This article is an open access article distributed under the terms and conditions of the Creative Commons Attribution (CC BY) license (<https://creativecommons.org/licenses/by/4.0/>).

Abstract: Aviation is one of the sectors affecting climate change, and concerns have been raised over the increase in the number of flights all over the world. To reduce the climate impact, efforts have been dedicated to introducing biofuel blends as alternatives to fossil fuels. Here, we report environmentally relevant data on the emission factors of biofuel/fossil fuel blends (from 13 to 17% *v/v*). Moreover, *in vitro* direct exposure of human bronchial epithelial cells to the emissions was studied to determine their potential intrinsic hazard and to outline relevant lung doses. The results show that the tested biofuel blends do not reduce the emissions of particles and other chemical species compared to the fossil fuel. The blends do reduce the elemental carbon (less than 40%) and total volatile organic compounds (less than 30%) compared to fossil fuel emissions. The toxicological outcomes show an increase in oxidative cellular response after only 40 min of exposure, with biofuels causing a lower response compared to fossil fuels, and lung-deposited doses show differences among the fuels tested. The data reported provide evidence of the possibility to reduce the climate impact of the aviation sector and contribute to the risk assessment of biofuels for aviation.

Keywords: biofuels; emission factors; *in vitro* exposure; hazard assessment; human exposure; aviation; climate change; air pollution

1. Introduction

Climate change is affecting the lives of populations all over the world. Expected increases in temperature are likely to be associated with increased mortality [1]. Furthermore, the environmental impacts of climate change on biodiversity, crop production, and animal habitats pose a serious threat to the planet as we know it [2–4].

To avoid such detrimental effects, governments have renewed their commitment by signing the Paris Agreement ([5]) which aims at limiting “global warming to well below 2, preferably to 1.5 degrees Celsius, compared to pre-industrial levels”. To achieve this goal, countries have agreed to reduce the emission of greenhouse gases and the extraction and consumption of fossil fuels.

The EU target to achieve carbon neutrality by 2050 requires action in several life, production, and societal sectors [6,7], with transport playing a relevant role [8]. Among the different sectors that use fossil fuels, aviation is the one which, in recent years, experienced the fastest growing rate [9]. Despite the improvements achieved in the last twenty years

to increase fuel efficiency, the aviation sector has faced a tremendous increase in the number of flights and passengers, becoming the EU's second largest greenhouse gas (GHG) emitter in the transport sector after road transport; in fact, the International Civil Aviation Organization (ICAO) estimated a potential three-fold increase in GHG emissions from the aviation sector from 2015 to 2050 [10].

Consequently, the EU have attempted (https://ec.europa.eu/clima/eu-action/transport-emissions/reducing-emissions-aviation_en accessed on 15 September 2022) to reduce the impact of this sector on climate change, acting at both the European and international levels.

Besides the emission of carbon dioxide (CO₂), aircrafts emit nitrogen oxides, soot, sulphate particles, and water [11]. These species influence cloudiness in the high atmosphere and hence solar radiation warming potential [12] and play a role in aerosol and ozone pollution in the troposphere, including at ground level [13].

To reduce the impact of aviation on the climate, great effort is being devoted to developing and testing fuel from renewable (therefore carbon-neutral) sources to substitute, partially or totally, the fossil fuels presently used [14,15]. Several different biofuels are currently available on the market, but hydroprocessed fatty acid esters and free fatty acid (HEFA) are considered the most promising for improving aviation carbon neutrality, although with some potential limitations to be considered [16]. Recently, the strict interplay between GHG emissions during fuel combustion and the energy demand of biofuel production has been reported, providing additional insight into the importance of considering the whole life cycle of the biofuel [17] when aiming at reducing production and emission costs. Laboratory tests conducted on different biofuel blends showed the capability of these fuels to reduce particle [18], CO, and NO_x [19] emissions. Similarly, a previous study [20] showed significant improvement in emissions with biofuel blends, findings confirmed also by inflight measurements. Notably, the most recent environmental report from the European Union Aviation Safety Agency (EASA [21]) clearly states that “European citizens are becoming increasingly aware of the affect that aviation activities have on their quality of life through climate change, noise and air quality...”.

Therefore, besides reducing climate change, the health risks associated with the replacement of conventional fuels with bio-based fuels should be considered. In fact, while diesel exhaust from on-road engines is a carcinogen for humans [22], less information is available for aircraft emissions and even less for the exhaust from biofuel for aviation. Several authors have reported an increase in air pollution near airports. Nanoparticle concentrations close to airports were higher than the concentrations recorded downtown near a major road [23], with relative increases as high as 28-fold near some airports [24]. Interestingly, Pirhadi et al. reported that the main activities influencing the air quality surrounding airports were take-off and landing [25]. Moreover, airport workers are particularly exposed to engine exhaust and, depending on the kind of task, ground workers are usually exposed to higher ultrafine particle concentrations [26] and experience higher lung-deposited doses than office or security workers [27]. Moreover, the emissions from airports strongly affects the populations living nearby, and significant correlations have been found between the onset of health issues and residence in the proximity of airports [28,29]. In agreement, toxicological evaluations of jet fuel vapors showed a relevant impact on the immune system [30], while in vitro studies of sampled airport emissions underlined in vitro effects comparable to diesel exhaust [31,32].

Surprisingly, in view of these data there is still a lack of information on the emission factors and the potential toxicological effects and human dosimetry of the emissions from aircraft engines run with biofuel blends. This assessment is pivotal to avoid contrasting offsets between climate change reduction requirements and air pollution and human protection needs. In this manuscript, we therefore aim at discussing this major aspect by accounting for the emission indexes and the toxicological impacts of exhaust from an airplane fueled with biofuel blends and a fossil fuel. We measured the emissions of the Rolls-Royce Spey engine, which is a low-bypass turbofan engine, installed on an AMX “Ghibli”, a military ground attack jet, provided by the Italian Air Force. The aircraft was

anchored to the ground and run with Jet A-1 synthetic fuel or different blends (13 and 17% HEFA in Jet A-1 fuel v/v, according to the safety requirements for the Air Force jet and personnel). The emissions were collected after preliminary mixing with the atmosphere and characterized for their physical and chemical properties. Moreover, the toxicological effects on BEAS-2B bronchial epithelial cells—exposed at the air–liquid interface to the emitted exhaust—and the human lung deposition, using the MPPD model, were determined to account for the potential hazard and the human exposure doses of the different fuels, thereby providing preliminary data for a risk assessment of the exhaust from different aviation fuels.

2. Materials and Methods

2.1. Sampling Line

Combustion emissions from an AMX fighter jet of the Italian Air Force equipped with a Spey engine (view Table 1 for more details) and fixed to the ground by means of a safety hook to avoid movement were collected at circa 20 m from the exhaust of the jet's Rolls-Royce Spey turbofan (Figure 1). The sampling line for the exhaust was composed of an aluminum pipe (diameter of 20 cm and length of 20 m), with the inlet placed at 110 cm from the ground, connected to a tubular expansion chamber of 6 m³ (diameter 120 cm, length 5 m). The expansion chamber was made of conductive antistatic polyethylene to avoid particle losses. The expansion chamber was then fixed to the roof of the Transportable Laboratory MINNI by means of a PVC net to avoid any possible movement by local winds. The emissions were sampled isokinetically using a controlled fan at the end of the sampling line (Figure 1). Four different sampling lines were placed in the expansion chamber and connected to the online monitors and instruments located in the transportable laboratory. Two consecutive experiments were performed with a fossil fuel (Jet A-1 type) and four consecutive tests after adding to the fossil fuel (Jet A-1 type) a selected quantity of a hydroprocessed fatty acid esters and free fatty acid (HEFA) biofuel (according to the specifics of Annex II ASTM D 7566). The final concentration of the HEFA fuel ranged between 13% (first and second tests) and 17% (third and fourth tests; chemical analysis of this blend is reported in Appendix B Table A1) v/v in the fossil fuel. Two different thrusts were used during each fuel test, 50% and 70% ($\pm 5\%$) of the maximal nominal power, while the final emission test (4th test with 17% biofuel) was performed at a higher thrust (60 to 95%) to empty the tank of the biofuel blend. The shift from the lower to the higher thrust during each test was announced by an acoustic signal and recorded for subsequent interpretation of the data.

Table 1. Specification of the Spey Mk 202 engine model used to test the different fuels.

Property	Prop. Info	Components	Comp. Info	Performance	Perf. Info
Type	Low-bypass turbofan	Compressor	Axial flow, 5-stage LP, 12-stage HP	Maximum thrust	54 kN, with reheat 91.2 kN
Length	5.2 m	Combustors	10 can-annular combustion chambers	Air mass flow	92.53 kg/s
Diameter	1.1 m			Specific fuel consumption	55.2 (g/kN)s with after burner, 17.8 (g/kN)s at military thrust
Dry weight	1856 kg	Turbine	2-stage LP, 2-stage HP	Thrust-to-weight ratio	5:1

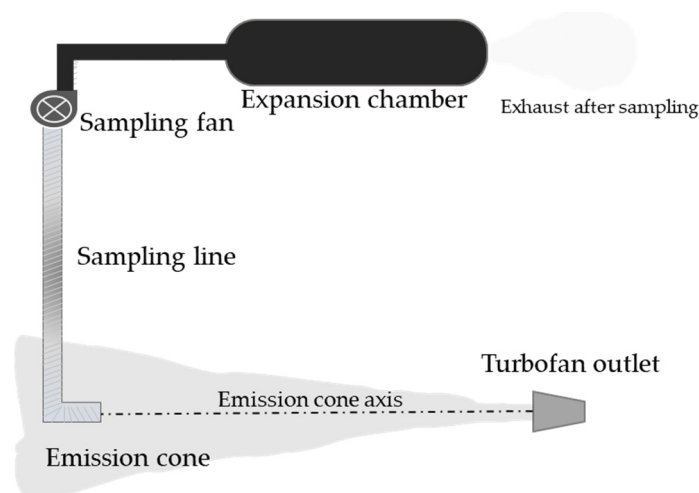


Figure 1. Schematic representation of the sampling line adopted to characterize the emissions from the Spey Mk 202 engine. The sampling inlet was placed in line with the axis of the exhaust emission cone. The suction of the emissions was performed by a sampling fan allowing a quasi-isokinetic sampling. The turbofan exhaust was then allowed to expand into an expansion chamber where instrument sampling lines were placed. The non-sampled exhaust was left to exit the expansion chamber during the whole sampling period.

2.2. Emission Characterization

Emissions originating from fossil or biofuel combustion were sampled in the expansion chamber and were characterized according to the following online monitors: total volatile non-methane organic compounds monitor (TNMHC, Synspec ALPHA 115); SO₂ monitor (TELEDYNE 101E H₂S/SO₂ Analyzer); NO₂/NO/NO_x monitor (2B Technologies Model 405 nm); CO₂ NDIR monitor (GO₃ Project Monitor O₃/CO₂); Scanning Mobility Particle Sizer, SMPS (TSI 3938 SMPS); Optical Particles Counter (OPC GRIMM mod. 1.107) for particle size distribution from 250 nm to 1.7 µm; SUNSET Semi-Continuous Carbon Aerosol Analyzer, with denuder to remove volatile organic compounds (for measuring total carbon—TC, organic carbon—OC, and elemental carbon—EC) according to the NIOSH-like thermal protocol; Aerosol Chemical Speciation Monitor (ACSM) for the detection in PM₁ of total organic matter (OA), ammonia (NH₄⁺), sulphate (SO₄²⁻), nitrate (NO₃⁻), and chloride (Cl⁻); Cultex[®] RFS Compact Type II module (CULTEX[®], Germany) for the direct exposure of in vitro lung models.

Besides the online monitors, three filter holders, connected to sampling pumps (Digit model, Zambelli, Italy, constant flow rate of 12.78 L/min), were used to collect exhaust samples for offline laboratory analyses. Pumps were switched on at the beginning of each test and switched off at the end to sample the separated test emissions, and a cyclone was used to select particles below PM_{2.5}. One filter holder was used to sample the exhaust on PTFE filters (Pall Teflon with ring pore size 1.0 µm and diameter 47 mm), and the two other filter holders were used to sample the exhaust on quartz filters (Pall 2500-QUAT-UP, diameter 47 mm). The PTFE filters were used to quantify the sampled mass by gravimetric determination and the metal and the trace element by XRF technique (ED-XRF, Rigaku NEX CG); one quartz filter was used to determine the amount of soluble ions (Cl⁻, NO₃⁻, SO₄²⁻, Na⁺, K⁺, NH₄⁺, Ca²⁺, Mg²⁺) by liquid ion chromatography (Dionex ICS 1100), while the other quartz filter was used to quantify the total carbon (TC), organic carbon (OC), and elemental carbon (EC) with a Dual-Optical Carbonaceous Analyzer (Sunset Laboratory, Tigard, OR, USA), as reported in [33]. The sampling line to assess TC was equipped with an additional backup quartz filter (quartz behind quartz filter, QBQ) [34,35] to account for the positive artefact caused by volatile compounds. A quarter of each quartz filter intended for the ions analyses was recovered and used for the analysis of PAHs associated with the exhaust (Supplementary materials and methods and Appendix B Table A2).

2.3. Emission Index Determination

The emission indexes from the fossil fuel and the biofuel blend were calculated for particle number, TNMHC, NO₂, SO₂, OC, and EC, accounting for interference factors that may have affected the dilution of the emissions at the exit of the turbofan, such as: the differences in meteorological variables (wind speed and wind direction), the different volume of the cone of emissions under different thrusts, and the slightly different alignment between the sampling line inlet and the emission cone axis.

The emission index (*EI*) represents the mass of emitted pollutant as a function of the mass of consumed fuel. To calculate the emission indexes for each pollutant, we assumed that all the mass of fuel was completely burnt during the test and that the measured CO₂ was apportionable only to the fuel burnt and its dilution in the atmosphere (*FD_{pr}*), in accordance with [36,37].

$$FD_{pr} = \left(\frac{EI_{CO_2}}{CO_{2pr}} \times C_{pr} \right) \times \frac{1}{V_r} \quad (1)$$

where *p* stands for the specific test, *r* stands for the RPM (thrust selected), *EI_{CO₂}* represents the total emission of CO₂, *CO_{2pr}* is the mean CO₂ concentration with the background value subtracted, while *C_{pr}* is the kilograms of fuel used in each test and under the selected thrust (after each test, the mass of fuel remaining in the AMX jet tanks was weighed), and, finally, *V_r* is the dilution volume for each RPM calculated according to Equation (2):

$$V_r = \left[\sum_{p=1}^n \left(\frac{EI_{CO_2}}{CO_{2pr}} \times C_{pr} \right) \right] \times \frac{1}{n} \text{ with } n = 5; r = 50\% \text{ or } 70\% \quad (2)$$

For the offline measurements, the subsequent correction factors were applied to account for different dilutions of the emissions:

$$FD_p = \left(\frac{EI_{CO_2}}{CO_{2p}} \times C_p \right) \times \frac{1}{V} \quad (3)$$

where *EI_{CO₂}* is the total emission of CO₂, and *CO_{2p}* is the measured carbon dioxide during a test *p* (for the filters, the samples of different thrust settings were pooled), while *C_p* is the mass of fuel used during a test *p*, and *V* is the dilution volume calculated according to Equation (4):

$$V = \left[\sum_{p=1}^n \left(\frac{EI_{CO_2}}{CO_{2p}} \times C_p \right) \right] \times \frac{1}{n} \text{ with } n = 5 \quad (4)$$

The emission index for the different parameters (*EI_x*) was then calculated according to [38] and Equation (5):

$$EI_x = \frac{x_{fd} \times S(x_{fd})}{CO_{2fd}} \times EI_{CO_2} \quad (5)$$

where *EI_{CO₂}* is the total mission index for CO₂ according to (1), *X_{fd}* and *CO_{2fd}* are the mass concentrations of the parameter *x* and of CO₂ with their background levels subtracted, while *S(x_{fd})* is a dimensional conversion factor.

2.4. Cell Culture and Exposure

Cell culture: Human bronchial epithelial cells (BEAS-2B, ECACC, Sigma-Aldrich, St. Louis, MI, USA) were maintained in LHC-9 medium (Thermo Fisher Scientific, Waltham, MA, USA) at 37 °C and 5% of CO₂.

One week before the exposure, cells were cultured at a density of 45.000 cells on the apical side of well inserts (Corning, 0.4 μm pore diameter, collagen-coated). The LHC-9 medium was changed every two days in both the apical and basolateral compartments. The day before the exposure, the apical medium was removed from all the inserts and cells were allowed to differentiate for 24 h (more details on the protocol in [39]).

Exposure condition: Online exposures to combustion exhaust of fossil fuel and biofuel blends were performed by means of two Cultex RFS modules. A sampling line, with a cyclone to select particles with an aerodynamic diameter smaller than 2.5 μm , was placed into the expansion chamber and directly connected to the exposure modules. In each module, three inserts were exposed directly to the combustion emissions, and three inserts were exposed to filtered air (for more detail, see [39]) and used as controls. At the end of the exposure, the cells and the medium in the basolateral compartment were recovered and directly manipulated according to the relative biological endpoints selected; for two experiments with the biofuel blend, a recovery of one hour was allowed, placing the cells into an incubator at 37 °C and 5% of CO₂ just after the end of the exposure. Exposure doses were calculated considering the number particle concentration measured by the SMPS and the OPC, these instruments being connected to the same sampling line of the exposure modules. For the toxicological test, exposure lasted for the complete duration (around 45 min) of each single emission test; therefore, emissions were collected at both 50 and 70% of thrust.

2.5. Toxicological Evaluation

Cell viability was assessed by measuring the LDH activity in the media recovered from control and exposed cells. Briefly, the recovered medium was diluted 1:1 *v/v* with CytoTox-One reagent (CytoTox-ONE™ Homogeneous Membrane Integrity Assay Promega, Madison, WI USA) and incubated for 10 min. The emissions of the conversion of the non-fluorescent resazurin to the fluorescent resorufin was measured in a fluorimeter (excitation λ 560 nm, emission λ 590 nm, Glomax Discover System, Promega, Madison, WI USA).

Inflammatory cytokines (IL-6, IL-8, IL-1 β , IL10, TNF- α , and IL-12) released in the medium underneath the cells were measured using the Human Inflammatory Cytokine CBA (Becton Dickinson, Franklin Lakes, NJ, USA) according to the manufacturer's instructions. Briefly, the medium from exposed and control cells, or the standards for the calibration curves, were mixed with the reaction beads and the antibodies stained with fluorescent phycoerythrin. After 3 h of incubation, the samples were read with a FACS Calibur (Becton Dickinson, Franklin Lakes, NJ, USA) and the pg/mL of the different cytokines determined according to the calibration curves.

Gene expression was assessed by extracting total RNA with the Quick-RNA Microprep Kit (Zymo Research, Irvine, CA, USA), according to the manufacturer's instructions. The amount and purity of the extracted RNA were evaluated using a fiber-optic Nanodrop ND-1000 spectrophotometer (Thermo Fisher Scientific, Waltham, MA, USA), calculating the 230/260 and 260/280 absorbance ratios. First-strand cDNA was synthesized using a high-capacity RNA-to-cDNA kit (Thermo Fisher Scientific, Waltham, MA, USA) according to the manufacturer's instructions. Analysis of the gene expression was carried out with quantitative real-time PCR (qRT-PCR) using SYBR Green master mix (Thermo Fisher Scientific, USA) and the following primers, as previously described: CYP1B1 [40], NQO1 [41], HO1 [42], IL-6 [43], and 18s [27]. qRT-PCR was performed on a StepOnePlus thermocycler (Thermo Fisher Scientific, USA) using the thermal cycling conditions consisting of a holding stage at 50 °C for 2 min and 95 °C for 10 min, followed by 40 cycles of each PCR step: (denaturation) 95 °C for 15 s and (annealing/extension) 60 °C for 1 min.

The relative fold change $2^{-\Delta\Delta\text{CT}}$ method was used to determine the relative quantitative gene expression compared with 18s as endogenous controls.

All PCR reactions were performed in triplicate and data were expressed as the mean \pm standard error (SE).

2.6. Human Exposure Assessment

Particle size number distributions from the different tests were used to quantify the potential maximal human lung-deposited dose with the MPPD 3.04 inhalation model. Five minutes of data were integrated into each test to obtain a mean particle number concentration. These mean values were used to calculate the deposition of the particles in the

trachea–bronchial and lung regions according to [39]. The model was run considering a 60 percent stochastic lung with a functional residual capacity of 3.3 L and an URT volume of 50 mL. Aerosol density was considered constant over the different size ranges and equal to 1 g/cm³ [44], and all the particles were modelled as perfect spheres. The variable exposure condition option was run considering the duration of each measurement as the time of exposure, nasal respiration, a tidal volume of 1250 mL, a breathing frequency of 20 inspirations per minute, and an inspiratory fraction of 0.5 with no pause. Deposition only, without clearance, was considered to obtain the integrated total mass deposited for each average diameter. Deposited doses in µg/cm² of the pulmonary or trachea–bronchial surfaces were calculated according to [45]. The reported calculations considered the emissions during the whole duration of each test, and therefore without separating emissions at 50% and 70% of thrust, to allow for comparison with the toxicological outcomes.

2.7. Statistical Analyses

Emission factors are reported as average and quadratic error to provide relevant intervals. Chemical characterization results are reported as mean and standard error. Biological results are reported as mean and standard deviation, and statistical significance was tested with ANOVA followed by post hoc analysis.

3. Results

3.1. Emission Characterization: Online Monitors

Volatile emissions are reported (Table 2) in terms of TNMHC, SO₂, NO₂, and CO₂ (µg or mg per m³), with the background levels already subtracted (Appendix B Table A3). Average emission concentrations (with the relative standard error) are reported for each fuel and for each thrust (RPM) tested. Higher TNMHC was observed during lower thrusts with a slightly higher, but not significant, increase in biofuel blends vs. the fossil fuel. NO₂, SO₂, and CO₂ emissions increased with the thrust applied, as expected from a better combustion efficiency. All gases showed a higher concentration during the biofuel combustions, but surprisingly higher were the values determined for SO₂, which were almost an order of magnitude higher. Notably, this difference is related to the sulfur content of the fossil fuel used to prepare the biofuel blends (Appendix B Table A1) and not to a direct effect of the biofuel per se.

Table 2. Emission concentrations (reported as mean with the relative standard error) for volatile compounds measured during the combustion tests after accounting for the dilution factor and background effect.

Fuel	Replica	RPM %	TNMHC mg/m ³	Std.err mg/m ³	SO ₂ µg/m ³	Std.err µg/m ³	NO ₂ µg/m ³	Std.err µg/m ³	CO ₂ mg/m ³	Std.err mg/m ³
Fossil	I	50	10.6	3.4	8.1	2.2	332	61	585	92
	I	70	9.8	4.7	14.9	1.4	710	146	1002	84
	II	50	10.2	2.4	5.6	1.8	316	54	478	124
	II	70	9.1	2.9	12.4	2.5	745	228	1057	219
Biofuel	I	50	10.9	2.5	105.7	9.1	467	100	687	212
	I	70	10.5	3.1	256.0	76.8	1231	210	1465	201
	II	50	16.9	3.2	209.5	60.0	697	278	788	293
	II	70	10.6	4.2	459.9	75.4	1521	190	1740	157
	III	50	19.4	4.5	406.0	86.5	826	175	1069	351
	III	70	13.7	4.9	662.6	72.8	1861	166	2004	121
	IV	60	12.0	3.3	234.6	41.9	519	204	621	142
	IV	95	7.7	1.6	455.5	68.6	1108	127	1334	139

The emissions of quasi-ultrafine (PM_{0.3}) and fine (PM_{0.3–1.7}) particles are reported, including the number particle concentration and relative mean geometric diameter for each fuel and thrust tested (Table 3), with the background effect already subtracted (the latter is

reported in Appendix B Table A4). The data show that the emission of particles increases (for PM_{0.3} and PM_{0.3–1.7}) with the thrust applied and that this higher emission is related to particles with a lower geometric mean diameter (GMD).

Table 3. Emissions for the fossil fuel and biofuel blends in terms of number of quasi-ultrafine (PM_{0.3}) and fine (PM_{0.3–1.7}) particles and the geometric mean diameter (GMD) after accounting for the dilution factor and background influence.

Fuel	Replica	RPM %	PM _{0.3} #/cm ³	Std.err #/cm ³	GMD nm	Std.err nm	PM _{0.3–1.7} #/cm ³	Std.err #/cm ³
Fossil	I	50	1.03 × 10 ⁶	3.20 × 10 ⁵	29.1	1.4	14.2	2.8
	I	70	1.66 × 10 ⁶	2.47 × 10 ⁵	23.3	1.5	23.1	5.5
	II	50	1.17 × 10 ⁶	2.01 × 10 ⁵	28.7	1.1	13.5	2.4
	II	70	2.00 × 10 ⁶	3.00 × 10 ⁵	22.9	2.4	25.8	10.6
Biofuel	I	50	2.62 × 10 ⁶	1.93 × 10 ⁵	24.0	1.2	13.0	2.9
	I	70	6.13 × 10 ⁶	8.14 × 10 ⁵	21.5	0.6	35.3	7.1
	II	50	3.54 × 10 ⁶	3.37 × 10 ⁵	22.6	1.0	22.0	5.7
	II	70	6.43 × 10 ⁶	2.52 × 10 ⁶	21.5	2.0	48.2	11.3
	III	50	5.24 × 10 ⁶	7.70 × 10 ⁵	23.4	1.0	23.7	5.6
	III	70	8.60 × 10 ⁶	2.88 × 10 ⁵	23.8	0.3	67.8	14.3
	IV	60	2.89 × 10 ⁶	5.12 × 10 ⁵	22.3	1.8	29.1	6.5
	IV	95	6.87 × 10 ⁶	5.69 × 10 ⁵	21.7	0.6	41.8	11.4

Similar increases were evident also for OC, EC, and TC (Table 4). Interestingly, the ratio of EC/OC was much higher for the fossil fuel at the lower thrust compared to the biofuel blends. The latter showed a lower ratio between EC and OC (always below 1), suggesting a remaining fraction of partially non-combusted organic species, in agreement with the TNMHC values. Background levels are reported in Appendix B Tables A5 and A6.

Table 4. Emission concentrations for OC, EC, and TC measured during the different tests—already accounting for the dilution factors and background effect—and the EC/OC ratio.

Fuel	Replica	RPM %	OC µgC/m ³	Std.err ±µgC/m ³	EC µgC/m ³	Std.err ±µgC/m ³	TC µgC/m ³	Std.err ±µgC/m ³	EC/OC
Fossil	I	50	28.6	6.9	48.1	6.9	76.7	20.3	1.68
	I	70	35.4	11.0	25.3	11.6	60.7	34.9	0.71
	II	50	24.9	8.3	59.1	7.4	106.3	31.8	2.37
	II	70	37.6	10.4	26.3	13.8	63.9	39.6	0.70
Biofuel	I	50	64.7	8.7	52.7	7.9	117.4	23.9	0.81
	I	70	102.4	11.8	66.2	8.9	168.6	30.0	0.65
	II	50	50.8	6.5	39.9	6.6	90.6	19.4	0.79
	II	70	126.6	14.6	66.4	11.6	193.0	40.7	0.52
	III	50	148.7	12.0	66.0	8.1	214.6	31.7	0.44
	III	70	154.6	17.7	52.1	10.8	206.7	49.3	0.34
	IV	60	101.3	9.8	37.2	6.2	138.5	27.4	0.37
	IV	95	95.2	13.4	32.9	8.4	128.2	38.5	0.35

3.2. Emission Characterization of Airborne Pollutants: Offline Analyses

Besides the online measurements, which allowed us to discriminate between different thrusts, offline filter analyses (sampling the emissions at different thrusts for each experiment) were carried out to characterize the emissions of selected chemical species. Here, we report the data for the ionic species and the metal and trace element species (data on PAHs, EC, and OC measured on the sampled filters are reported in Appendix B Tables A2 and A6, respectively). Airborne mass concentrations of the ionic species (Table 5) showed higher values for nitrate (NO₃⁻) and nitrite (NO₂⁻) during fossil fuel combustion compared to

the biofuel blends that, on the contrary, were characterized by higher concentrations of sulfate (SO_4^{2-}).

Table 5. Airborne concentration of ionic species measured on filters collected during the different tests. Data are reported as average and standard error ($n > 2$). Concentrations below the detection limit of the technique are reported in the table as nd (not detected). Blank cells represent missing values.

Fuel	Replica	NO_2^-	Std.err	NO_3^-	Std.err	SO_4^{2-}	Std.err	NH_4^+	Std.err
		$\mu\text{g}/\text{m}^3$	$\pm\mu\text{g}/\text{m}^3$	$\mu\text{g}/\text{m}^3$	$\pm\mu\text{g}/\text{m}^3$	$\mu\text{g}/\text{m}^3$	$\pm\mu\text{g}/\text{m}^3$	$\mu\text{g}/\text{m}^3$	$\pm\mu\text{g}/\text{m}^3$
Fossil	I	36.0	1.0	7.5	0.4	0.35	0.01	nd	nd
	II					0.42	0.03	nd	nd
Biofuel	I	6.1	0.6			1.0	0.2	nd	nd
	II					1.9	0.3	0.43	0.03
	III					1.5	0.2	0.38	0.02
	IV			2.1	0.5	3.5	0.4	1.48	0.05
Background		0.114	0.003	0.71	0.08	0.79	0.04		

The concentrations of the ionic species were also measured in the QBQ filters (Table 6), which showed that these chemical species partitioned between the two filters during the sampling. In this case, the differences observed between the two fuels are less evident, and a slight increase in the average content of nitrite in the biofuel samples ($15.00 + 0.34$) compared to the fossil fuel ($9.80 + 0.25$) was measured.

Table 6. Ionic species concentration in the QBQ filters. Data are reported as average ($n > 2$) and standard error. Concentrations below the detection limit of the technique are reported in the table as nd (not detected).

Fuel	Replica	NO_2^-	Std.err	NO_3^-	Std.err	SO_4^{2-}	Std.err	NH_4^+	Std.err
		$\mu\text{g}/\text{m}^3$	$\pm\mu\text{g}/\text{m}^3$	$\mu\text{g}/\text{m}^3$	$\pm\mu\text{g}/\text{m}^3$	$\mu\text{g}/\text{m}^3$	$\pm\mu\text{g}/\text{m}^3$	$\mu\text{g}/\text{m}^3$	$\pm\mu\text{g}/\text{m}^3$
Fossil	I	15.8	0.3	7.8	0.4	17	0.4	nd	nd
	II	3.8	0.2	7	1	18	1	nd	nd
Biofuel	I	2.12	0.09	7	1	17	2	nd	nd
	II	13.7	0.3	9	1	18	0.4	nd	nd
	III	33.2	0.7	17.9	0.4	21	0.5	nd	nd
	IV	11.0	0.3	5.9	0.3	13	0.3	nd	nd
Background		7.34	0.2	4.3	0.2	8.7	0.7	nd	nd

The metal and elemental species determined by XRF showed similar concentrations between the fossil fuel and biofuel blends during the different replica. A relative increase in the concentration of antimony and barium was evident in the fossil fuel emission sample, but this increase was not significant (Appendix B Table A7).

3.3. Emission Indexes

The possibility to compare the relative emissions of the two fuels (fossil fuel vs. biofuel blends) was also explored by determining the specific emission indexes per unit of fuel burnt during the tests (Table 7). The emission indexes per unit of fuel (Kg) showed that the biofuel blends were higher emitters of particles in the ultrafine mode (a diameter below 100 nm) and partly in the accumulation mode (roughly, the diameter was between 100 and 300 nm). Biofuels also increased the release of NO_2 and OC, and the other parameters were comparable among the two fuels. Again, the SO_2 higher emission index should not be considered as representative of the biofuel blends but as an artefact due to the properties of the fossil fuel used to prepare the blends. Similar results were obtained from the sampling

on filters (Appendix B Table A8) which also showed a reduced emission index for biofuel blends when considering nitrite and nitrate emissions and for the metal and trace elements detected.

Table 7. Emission indexes calculated per kg of fuel consumed during each test, grouping the experiments with thrust equal to 50% and with thrust equal to 70%.

	Biofuel Blend		Fossil Fuel		Ratio Bio/Fossil	
	50%	70%	50%	70%	50%	70%
	Average (quadratic error)	Average (quadratic error)	Average (quadratic error)	Average (quadratic error)	Average (quadratic error)	Average (quadratic error)
Total particle number $D_p > 7\text{nm}$ (#/Kg)	1.4×10^{16} (2.6×10^{15})	1.4×10^{16} (2.6×10^{15})	6.4×10^{15} (2.3×10^{15})	5.6×10^{15} (1.2×10^{15})	2.2	2.3
Total nanoparticles $D_p < 40\text{ nm}$ (#/Kg)	1.2×10^{16} (2.2×10^{15})	1.2×10^{16} (2.2×10^{15})	4.5×10^{15} (1.6×10^{15})	4.5×10^{15} (1.2×10^{15})	2.6	2.6
Total ultrafine particles $40 < D_p < 100\text{ nm}$ (#/Kg)	2.1×10^{15} (7.6×10^{14})	2.1×10^{15} (7.6×10^{14})	1.6×10^{15} (6.8×10^{14})	9.1×10^{14} (2.7×10^{14})	1.4	1.1
Accumulation-mode particles $100 < D_p < 300\text{ nm}$ (#/Kg)	1.4×10^{14} (4.6×10^{13})	1.4×10^{14} (4.6×10^{13})	1.2×10^{14} (3.5×10^{13})	1.0×10^{14} (4.5×10^{13})	1.1	0.7
PM _{0.3} , $D_p > 300\text{ nm}$ (#/Kg)	7.3×10^{10} (5.8×10^{10})	7.3×10^{10} (5.8×10^{10})	8.0×10^{10} (4.4×10^{10})	7.5×10^{10} (3.0×10^{10})	0.9	1.2
TNMHC (g/Kg)	58.5 (22.0)	58.5 (22.0)	60.1 (23.8)	28.9 (16.7)	1	0.7
NO ₂ (mg/Kg)	2460.4 (1229.2)	2460.4 (1229.2)	1867.5 (470.5)	2225.0 (820.4)	1.3	1.3
SO ₂ (mg/Kg)	842.4 (309.4)	842.4 (309.4)	39.1 (16.4)	41.9 (9.3)	21.6	19.3
OC (mgC/Kg)	313.6 (63.7)	313.6 (63.7)	153.7 (63.2)	111.7 (46.3)	2.0	2.1
EC (mgC/Kg)	199.1 (50.8)	115.2 (34.8)	312.8 (59.7)	78.9 (55.0)	0.6	1.5

3.4. Toxicological Effects

Direct exposure to the airborne emissions from the differential combustion of the fossil fuel and biofuel blends aimed at determining whether, besides possible chemical and physical differences among the emissions from the two fuels, contrasting effects were accountable when focusing on the acute responses of the lung epithelia.

The exposure doses calculated for the in vitro models (Table 8) showed higher maximal deposition during the experiments with the biofuel blends. The third experiment with the biofuel blend showed the highest exposure doses compared to the other fuels. Interestingly, biofuel blend exposures were characterized by a higher contribution of deposited UFP mass compared to the fossil fuel ones, which accounted for the higher number of these particles emitted during the biofuel tests.

Cell viability showed no significant differences among the treated and control groups (data not shown). The cytokine panel, characterized in the collected cell media, showed that no quantifiable proteins were detectable right after the exposure; only after 1 h of recovery from the exposure was the IL-6 quantified in the medium underneath the cells, but no statistical difference was reported between the control (13.8 pg/mL + 4.6 pg/mL) and exposed cells (12.4 pg/mL + 1.4 pg/mL, biofuels after 1 h recovery). The analysis of the expression of a set of selected genes also showed slight (not statistically significant) changes between the groups, except for the HO1 gene (Figure 2). By grouping all the samples, HO1 was statistically increased after the exposure to both the fossil fuel and the bio-blend emissions compared to the control cells, with the highest gene expression increase demonstrated in response to the fossil fuel exposures. In fact, both of the exposures with

the fossil fuel significantly increased the expression of HO1 (Appendix B Figure A1), while minor non-significant variations were observed for all other genes. In comparison, the exposure to biofuel blend emissions (Appendix B Figure A2, panel a,b) showed a significant gene expression increment but with a lower magnitude. Interestingly, after 1 h recovery, the relative increase in HO1 expression in biofuel-exposed cells (Appendix B Figure A2, panel c,d) increased dramatically, thus suggesting that the oxidative effects triggered by the emissions drive an acute and significant effect on human lung cells.

Table 8. In vitro model doses of exposure. Doses are reported as number of particles and mass of particles deposited per square cm of cell surface. The relative contribution of ultrafine particles (UFP, particles with diameter < 100 nm) is also reported.

Fuel	Replica	Exposure Dose (#/cm ²)			Exposure Dose (µg/cm ²)		
		Total PM Dose	UFP Dose	UFP/PM	Total PM Dose	UFP Dose	UFP/PM
Fossil	I	1.38×10^5	1.38×10^5	0.995	2.47×10^{-6}	1.75×10^{-6}	0.709
	II	1.68×10^5	1.67×10^5	0.996	2.66×10^{-6}	1.96×10^{-6}	0.738
Biofuel	I	5.38×10^5	5.37×10^5	0.998	5.21×10^{-6}	4.31×10^{-6}	0.827
	II	6.14×10^5	6.14×10^5	0.998	5.85×10^{-6}	4.91×10^{-6}	0.840
	III	6.79×10^5	6.78×10^5	0.998	7.46×10^{-6}	6.52×10^{-6}	0.873
	VI	6.30×10^5	6.30×10^5	0.999	5.00×10^{-6}	4.46×10^{-6}	0.892

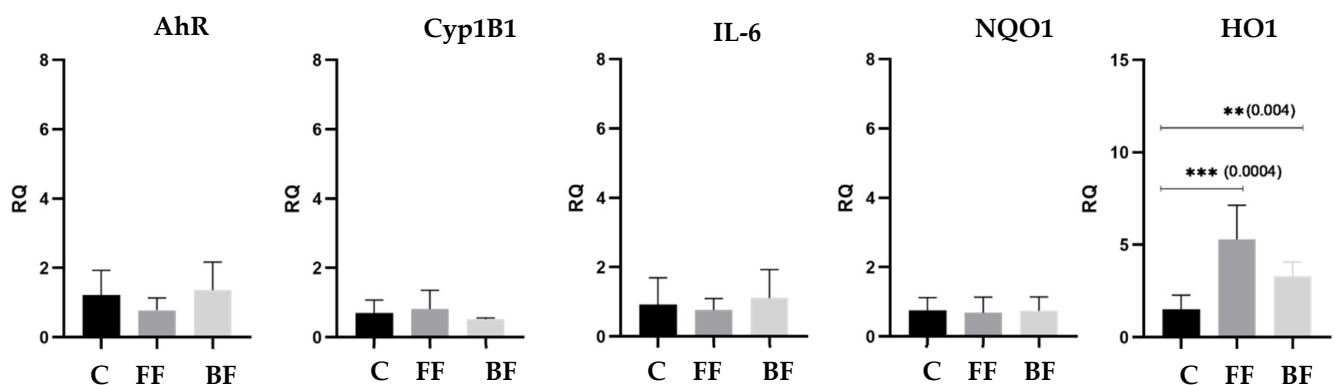


Figure 2. Differential gene expression after exposure to filtered air (C), fossil fuel emissions (FF), and biofuel blend emissions (BF).

3.5. Human Exposure

Potential human exposure calculated with the MPPD model showed (Table 9) higher lung-deposited doses during the biofuel tests. Interestingly, the size-resolved depositions (Figures 3 and 4) of the two sets of experiments showed some differences. Fossil fuel deposition was dominated by a main peak of particles with a diameter of around 80 nm, while biofuel blends were characterized by a distribution with two peaks, the first referring to particles with a diameter of around 30 nm and the second around 80 nm. All the experiments showed depositions well above the background level within 300 nm of particle diameter. After this, the background particles were affecting the deposition doses in all the experiments, suggesting that the emissions from the jet were characterized by particles below 300 nm.

Table 9. Deposited doses of particles during emission tests and during background monitoring. Data are reported as deposited mass ($\mu\text{g}/\text{cm}^2$) of trachea-bronchial (TB) or pulmonary (P) epithelial surface.

Fuel	Replica	TB Deposition ($\mu\text{g}/\text{cm}^2$)	P Deposition ($\mu\text{g}/\text{cm}^2$)
Background	I	2.43×10^{-6}	3.09×10^{-8}
Fossil	I	1.61×10^{-5}	2.41×10^{-7}
	II	1.69×10^{-5}	2.57×10^{-7}
Biofuel	I	3.18×10^{-5}	5.00×10^{-7}
	II	6.90×10^{-5}	1.09×10^{-6}
	III	1.07×10^{-4}	1.72×10^{-6}
Background	II	2.54×10^{-6}	3.36×10^{-8}

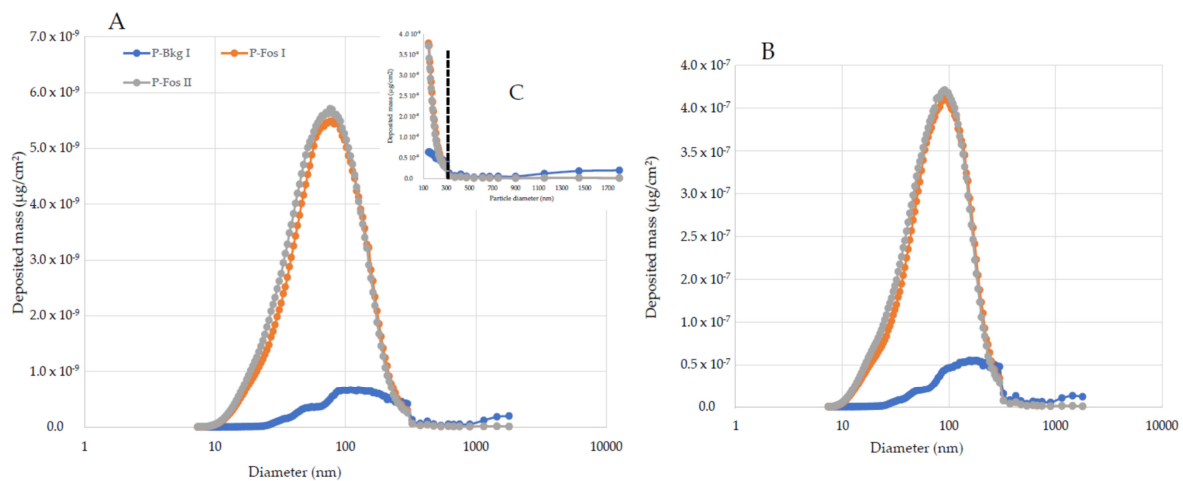


Figure 3. Pulmonary deposition of fossil fuel emissions (P-Fos I and P-Fos II) emitted, and the background (P-Bkg I) particles for the pulmonary (A) and trachea-bronchial (B) regions. Maximal contribution of emission is within 300 nm (C), after which background particulate distribution accounts for the measured deposition. One maximal peak of deposition (80 nm) is evident.

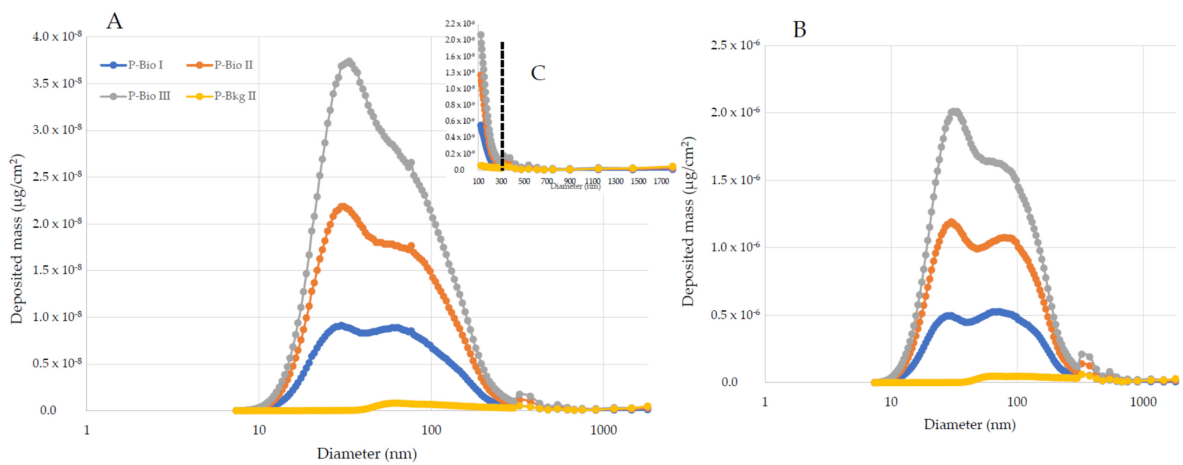


Figure 4. Pulmonary deposition of biofuel blends emitted (P-Bio I to III), and the background (P-Bkg II) particles for the pulmonary (A) and trachea-bronchial (B) regions. Maximal contribution of emission is within 300 nm (C), after which background particulate distribution accounts for the measured deposition. Two peaks of deposition are reported, one at 30 nm and one at around 80 nm.

4. Discussion

Reducing the impact of anthropogenic activities on climate change is the most important environmental issue if the present generations want to maintain the equilibrium of the several processes that allow life on earth [46].

The aviation sector impacts climate change due to its massive use of fossil fuels [47,48] and the steadily increasing number of flights recorded in the last few decades [9]. In recent years, several research groups have reported data on the potential benefit of reducing the use of fossil fuels by substitution with biofuel blends. Dray et al. [48] reported a significant benefit in terms of CO₂ equivalent [49] by substituting the fuels of fossil origin with cellulosic biomass-derived fuels. More recently, Staples et al. [50] enlarged the study comprising different feedstock sources to produce alternative aviation fuels, providing additional evidence for a potential reduction in GHG emissions from the aviation sector. In addition, the use of biofuel has been shown to reduce not only climate-changing emissions but also particulate emissions [44,51–53], which in turn might improve the climate by reducing the formation of contrail cloudiness [54]. Our results are in line with these previous results and provide additional evidence for the emission factors and the potential health impact of emissions from a jet fueled with a reference fossil fuel and different blends of biofuel and the fossil fuel. In fact, the reduction in volatile organic compounds (TNMHC) and elemental carbon (EC) is in line with previous results [18,22,55]. On the contrary, other parameters (fine and ultrafine PM number concentration, OC, and NO₂) show a surprising increase, although similar emission factors have been reported for commercial flights [56]. These data are, however, related to the chemical properties of the Jet A-1 fossil fuels used (Appendix B Table A1) rather than to the biofuel blends. The relevance of sulfur in modifying the emission factors agrees with the factors reported by [20] and [57,58] that showed the particles' emission indexes varying by two orders of magnitude, with higher emission values affected by the higher sulfur content.

In addition, the variation in the ratio between EC and OC that we also report here (Table 3) agrees with the data from Moore and co-workers [20] that showed a reduction in the emission of black carbon at a higher fuel flow rate in the jet engine, while the emission of organic compounds was less related to the fuel flow rate. Our data, accordingly, show that at the highest thrust tested (almost 95%) the concentration of EC in µgC/m³ is around half of the concentrations measured at lower thrusts.

Ultrafine particles are a major environmental concern in areas close to major airports [24,25]. The values recorded and here reported are in perfect agreement with those reported by [59]. In fact, the authors report occupational exposures to ultrafine particles as high as 10⁶–10⁷ particles per cm³. Notably, Michaelis et al. [60] recently showed that values for the in-cabin measurement of UFP can vary in the order of 10⁴ to 10⁵ particles/cm³. Ren et al. [61] demonstrated that the in-cabin values were highly related to the take-off operations in airplanes waiting, before departure, in areas downwind the take-off area.

The potential impact of aviation emissions on human health is in fact a subject of great debate [13]. Berret et al. [62] reported a significant impact of aviation emissions on mortality. Cavallo et al. [63] outlined the potential genotoxic effects of airport emissions in exposed workers, while the potential formation of ozone from aircraft emissions has been recently related to mortality and skin cancer [64]. Here, we showed that biofuel has a lower capability to induce acute epithelial lung response (lower expression of the oxidative protection gene, HO1) compared to fossil fuel. Notably, the recovery of exposed cells for just one hour induced a dramatic increase in HO1 expression. Nonetheless, the increase in the heme-oxygenase gene reported here is in line with a recent paper [65,66] suggesting that the activation of this gene protects against the adverse effects of air pollution. Interestingly, the activation of this gene has also been described by [31] after 24 h of exposure to airplane emissions at 85% or ground-idle thrusts (controlled using the engine combustor inlet temperature and not, as in our experiments, by actually increasing the airplane thrust) as showing a reduction in biofuel (32% *v/v* HEFA/Jet A-1) HO1 induction. Moreover, 90 days of exposure of mice to airport samples was reported to induce significant lung damage [67].

The lung-deposited mass doses, considering the short time of exposure defined by the experimental approach, agree with the expected particle deposition reported by other authors (summarized in [68]) and during combustion events such as forest burning [69].

In conclusion, we report novel data on the possibility of using biofuels to improve sustainability in the aviation sector: biofuel blends should therefore be considered to reduce CO₂ emissions from the aviation sector. Our emission factors clearly showed that a refinement of the Jet A-1 requirements may be relevant for the reduction in SO₂.

The data agree with those previously reported and add a first preliminary evaluation of the hazard of aircraft emissions and the expected lung doses. These data improve our understanding of the exposure doses of people living in proximity of, or working in, an airport and also underline the importance of assessing the health impact of biofuel blends, at least on the respiratory system. In fact, our data show that acute exposure to fossil fuel and biofuel blends might cause an oxidative burst in lung tissue and that the expected deposited doses in human lungs increase with the content of the biofuel in the blend. Significantly, biofuel determines the deposition of ultrafine particles of 30 nm.

Significant improvement in the sustainability of the aviation sector may be obtained by biofuels, possibly reducing at the same time the potential health effects on exposed populations, although additional investigation should be devoted to better understand the impacts on health of biofuel blend emissions, possibly considering sub-chronic exposures and the use of biological models representative of other potential target tissues.

Author Contributions: M.G.: in vitro exposure experimental campaign, conceptualization, realization, data analysis, human dosimetry, and manuscript drafting and reviewing; M.B. (Berico Massimo): conceptualization, realization, installation of the sampling framework, supervision of the experimental campaigns, data analysis, and manuscript revision; M.G.G.: in vitro exposure and biological test realization, data analyses, and manuscript revision; G.C.: offline filter analyses, data analyses, manuscript revision; T.L.T.: offline filter analyses, data analyses, manuscript revision; A.M.: offline filter analyses, data analyses, experimental campaign realization, manuscript revision; E.P.: data analyses and manuscript revision; M.S. (Stracquadiano Milena): offline filter analyses, data analyses, experimental campaign realization, manuscript revision; M.S. (Santoro Massimo): gene expression analyses and manuscript revision; B.B.: in vitro biological analyses, supervision, and manuscript revision; A.P.: manuscript writing and revision and data analysis; A.C.: experimental campaign supervision, military operational supervision, on-site logistic supervision, biofuel blending management, ground tests, engine coordination and organization, manuscript revision; M.B. (Bernabei Manuele): experimental campaign supervision, military operational supervision, on-site logistic supervision, biofuel blending management, ground tests, engine coordination and organization, manuscript revision; G.Z.: experimental campaign realization, idealization of the experimental framework, and manuscript revision. All authors have read and agreed to the published version of the manuscript.

Funding: The present activities have been funded by the Italian Ministry for Environment (D.D. 367/CLE 23/12/2016).

Institutional Review Board Statement: Not applicable for this study.

Informed Consent Statement: Not applicable for this study.

Data Availability Statement: Not applicable.

Acknowledgments: The authors would like to acknowledge all the personnel of the Italian Air Force of Pratica di Mare that allowed the realization of these experiments. The authors warmly acknowledge Luisealla Ciancarella and Francesca Pacchierotti for supporting personnel at ENEA (Bologna and Rome research centers) during the different steps of this experimental work. The authors are also grateful to Giuseppe Raschellà, Eugenia Cordelli, and Patrizia Eleuteri (ENEA, Rome) for their precious assistance with ALI exposure, and to Salvatore Chiavarini (ENEA, Rome) for PAH analysis.

Conflicts of Interest: The authors declare no conflict of interest.

Appendix A

Supplementary materials and methods for Appendix B Table A2. The quarters of filters were pooled according to the fuel they derived from to obtain two distinct pools, one for the fossil fuel and one for the biofuel. The pools were subjected to an accelerated solvent extraction (ASE 200 Dionex) in a low-volume vial (7 mL) with the following settings: extraction solvent hexane/acetone 1:1, T extraction 120 °C at 1500 psi, two consecutive extraction cycles with 5 min of static phase. Since the extracts were also prepared for subsequent toxicological analysis (not reported here), the filters were not spiked with reference materials to avoid possible contamination or formation of artefacts. At the end of the extraction, circa 10% in weight of the extract was recovered, spiked with deuterated reference compounds (anthracene-d10, pyrene-d10, crysene-d12, perylene-d12), dried to a final volume of 150 µL, and subjected to GC-MS for PAH quantification.

GC/MS (Agilent 7890a GC/5975c MS) equipped with a capillary column DB-5ms (Agilent, 30 m × 250 µm × 0.25 µm) was run with the following thermal program: 40 °C for two min, 20 °C/min up to 200 °C and then rest for 1 min, 4 °C/min up to 300 °C and then rest for 1min, 20 °C/min to reach 320 °C and then rest for 7 min, ionization at 70 eV, and data acquisition in Single Ion Monitoring (SIM).

Appendix B

Table A1. Chemical and physical characterization of bio-blend fuel 17% and content of sulfur in the bio-blend and fossil fuels used for reference test and blend tests.

Parameter	Limit Values for Jet A-1 Fuel Type		Value	Test Method
	Reference Values			
Color	none		+28	ASTM D 156
Density at 15 °C (Kg/m ³)	775.0–840.0		793.3	ASTM D4052
Distillation initial point (°C)	none		158	ASTM D86
Distillation initial point (10%) (°C)	≤205		173	ASTM D86
Distillation initial point (50%) (°C)	none		198	ASTM D86
Distillation initial point (50%) (°C)	none		236	ASTM D86
Distillation final point (°C)	≤300		262	ASTM D86
Distillation residual (% volume)	≤1.5		1.0	ASTM D86
Distillation losses (% volume)	≤1.5		0.8	ASTM D86
Viscosity at 20 °C (cSt)	≤8.0		3.9	ASTM D445
Flash point (°C)	≥38		45	ASTM D56
Thermal stability at 260 °C: pressure drop (mmHg)	≤25		0	ASTM D3241
Thermal stability at 260 °C: deposit thickness (nm)	≤85		5	ASTM D3241
Aromatic hydrocarbons (mL/100mL)	≤25.0		16.7	ASTM D1319
Doctor test	negative		negative	ASTM D4952
Corrosion on copper lamina (n)	≤1		1	ASTM D130
Lower calorific value (MJ/Kg)	≥42.80		43.20	ASTM D3338
Smoke point (mm)	≥19		25	ASTM D1322
Total acidity (mg KOH/g)	≥0.015		<0.015	ASTM D3242
Electric conductivity (pS/m)	50–600		90	ASTM D2624
<i>TOTAL SULFUR CONTENT:</i>				
Total sulfur in the bio-blend 20% (g/100 g)	≤0.3		0.0928	ASTM D4294
Total sulfur in the fossil fuel used for the blend (g/100 g)	≤0.3		0.1175	ASTM D2622
Total sulfur in HEFA fuel (g/100 g)	≤0.0015		0.0012	ASTM D2622
Total sulfur in the fossil fuel used for the first two reference tests (g/100 g)	≤0.3		0.07	ASTM D4294

Table A2. Airborne concentration of PAHs measured on quartz filters. Values are reported as average and standard deviation pooling the whole filter obtained during the fossil fuel and biofuel tests.

PAH	Fossil Fuel		Biofuel Blend	
	ng/m ³	±ng/m ³	ng/m ³	±ng/m ³
Phenanthrene	60.5	6.1	28.9	2.9
Anthracene	6.3	0.6	6.1	0.6
Fluoranthene	109.5	10.9	121.4	12.1
Pyrene	84.8	8.5	146.7	14.7
Benzo[a]anthracene	92.3	9.2	54.6	5.5
Chrysene	145.2	14.5	116.4	11.6
Benzo[b+j]fluoranthene	363.6	36.4	314.0	31.4
Benzo[k]fluoranthene	152.0	15.2	126.2	12.6
Benzo[a]pyrene	324.8	32.5	277.0	27.7
Indeno[1,2,3-cd]pyrene	407.4	40.7	323.3	32.3
Dibenzo[a,h]anthracene	17.0	1.7	16.3	1.6
Benzo[ghi]perylene	473.6	47.4	415.5	41.6

Table A3. Volatile compounds' emission indexes (in unit mass per cubic meter) measured during background monitoring.

Fuel	TNMHC mg/m ³	Std mg/m ³	SO ₂ µg/m ³	Std µg/m ³	NO ₂ µg/m ³	Std µg/m ³	CO ₂ mg/m ³	Std mg/m ³
Fossil	2.3	0.6	6.6	1.1	27	10	1046	139
	2.5	0.4	8.1	0.9	25	6	1015	95
Biofuel	1.9	0.7	6.4	0.7	24	6	998	55
	2.2	0.5	8.9	0.8	19	11	983	54
	2.1	0.7	6.2	1.2	27	7	976	109

Table A4. Particulate matter emission indexes (number of particles-#/per cubic cm) measured during background monitoring.

Fuel	Replica	PM _{0.3} #/cm ³	std #/cm ³	PM _(0.3-1.7) #/cm ³	std #/cm ³
Fossil	I	5522.5	741.6	18.4	2.3
	II	5517.8	643.9	14.2	1.6
Biofuel	I	7258.7	3025.7	21.4	2.2
	II	6645.5	2768.5	24.6	2.0
	III	7452.4	2444.7	22.8	3.2
	IV	8873.7	1391.3	37.7	3.8

Table A5. Carbon species (OC, EC, and TC) measured during background monitoring. The data are reported as average for the whole fossil fuel and biofuel blend tests. Only biofuel test IV is reported separately.

Fuel	OC µgC/m ³	err ± µgC/m ³	EC µgC/m ³	err ± µgC/m ³	EC/OC
Fossil	9.7	1.0	3.4	0.3	0,35
Biofuel	6.9	0.7	1.8	0.2	0,26
Biofuel IV	8.6	0.9	6.5	1.1	0,76

Table A6. Concentrations of total PM_{2.5}, EC, OC, and total measured PAHs in filters sampled during the different replica. Data are reported as average and the relative error.

Fuel	Replica	PM _{2.5} µg/m ³	err ±µg/m ³	EC µgC/m ³	err ±µgC/m ³	OC µgC/m ³	err ±µgC/m ³	EC/OC	PAHs µg/m ³	err ±µg/m ³
Fossil	I	112.6	7.0	44.0	5.8	25.2	3.5	1.75	2.2	0.2
	II	141.8	8.6	51.4	6.7	36.7	5.0	1.40	2.3	0.2
Biofuel	I	241.0	16.0	69.9	8.7	69.7	9.3	1.00	1.9	0.2
	II	322.8	21.3	64.8	8.2	100.1	16.0	0.65	1.6	0.2
	III	290.2	19.3	65.8	8.4	143.5	19.0	0.46	2.4	0.2
	IV	154.2	8.9	38.4	8.3	65.4	8.7	0.59	1.6	0.2
Background	Fossil	19.5	1.0	3.4	0.3	9.7	1.0	0.35		
	Bio I-III	16.5	1.0	1.8	0.2	6.9	0.7	0.26		
	Bio IV	27.0	1.4	6.5	1.1	8.6	0.9	0.76		

Table A7. Concentration of metals during the different tests. Data are reported as average and the relative error.

Fuel	Replica	V		Cr		Ni		Sb		Ba	
		µg/m ³	err	µg/m ³	err	µg/m ³	err	µg/m ³	err	µg/m ³	err
Fossil	I	0.0025	0.0004	0.12	0.01	0.08	0.01	0.12	0.02	1.0	0.1
	II	0.0023	0.0004	0.11	0.01	0.021	0.003	0.13	0.03	1.26	0.07
Biofuel	I	0.0051	0.0008	0.11	0.01	0.048	0.008	0.085	0.008	0.29	0.03
	II	0.004	0.001	0.103	0.009			0.08	0.01	0.68	0.09
	III	0.007	0.001	0.126	0.006			0.11	0.02	0.87	0.07
	IV			0.086	0.007			0.042	0.005	0.42	0.03

Table A8. Emission indexes obtained from filter samples: data are reported as average for each fuel with the relative quadratic error in brackets.

	Biofuel Blends	Fossil Fuel	Ratio Biofuel vs. Fossil
PM _{2.5} mg/Kg	612.0 (70.4)	455.6 (39.5)	1.3
OC mgC/Kg	219.7 (54.1)	109.9 (21.4)	2.0
EC mgC/Kg	145.6 (31.8)	169.4 (31.5)	0.9
PAHs mg/Kg	4.2 (2.5)	8.0 (3.9)	0.53
NO ₂ ⁻ mg/Kg	5.1 (0.5)	65 (4)	0.08
HONO mg/Kg	4.8 (0.6)	0.9 (0.1)	5.4
NO ₃ ⁻ mg/Kg	0 (0)	12.3 (3.6)	-
HNO ₃ mg/Kg	4.2 (0.8)	6.7 (2.4)	0.6
SO ₄ ²⁻ mg/Kg	3.1 (0.5)	1.4 (0.1)	2.3
H ₂ SO ₄ mg/Kg	20 (4)	27 (3)	0.7
NH ₄ ⁺ mg/Kg	0.80 (0.08)	-	-
V mg/Kg	0.010 (0.001)	0.008 (0.0005)	1.3
Cr mg/Kg	0.12 (0.02)	0.21 (0.03)	0.57

Table A8. Cont.

	Biofuel Blends	Fossil Fuel	Ratio Biofuel vs. Fossil
Ni mg/Kg	0.07 (0.02)	0.1 (0.02)	0.7
Sb mg/Kg	0.11 (0.02)	0.28 (0.07)	0.39
Ba mg/Kg	0.4 (0.1)	2.8 (0.7)	0.25

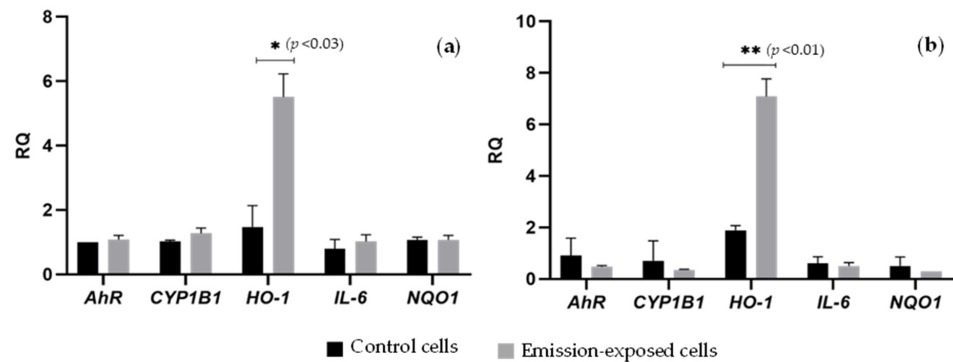


Figure A1. Gene expression of selected genes during the two exposures to fossil fuel emissions. Fossil I (a) and fossil II (b) emissions caused similar gene expression variation. All the other genes were not modified.

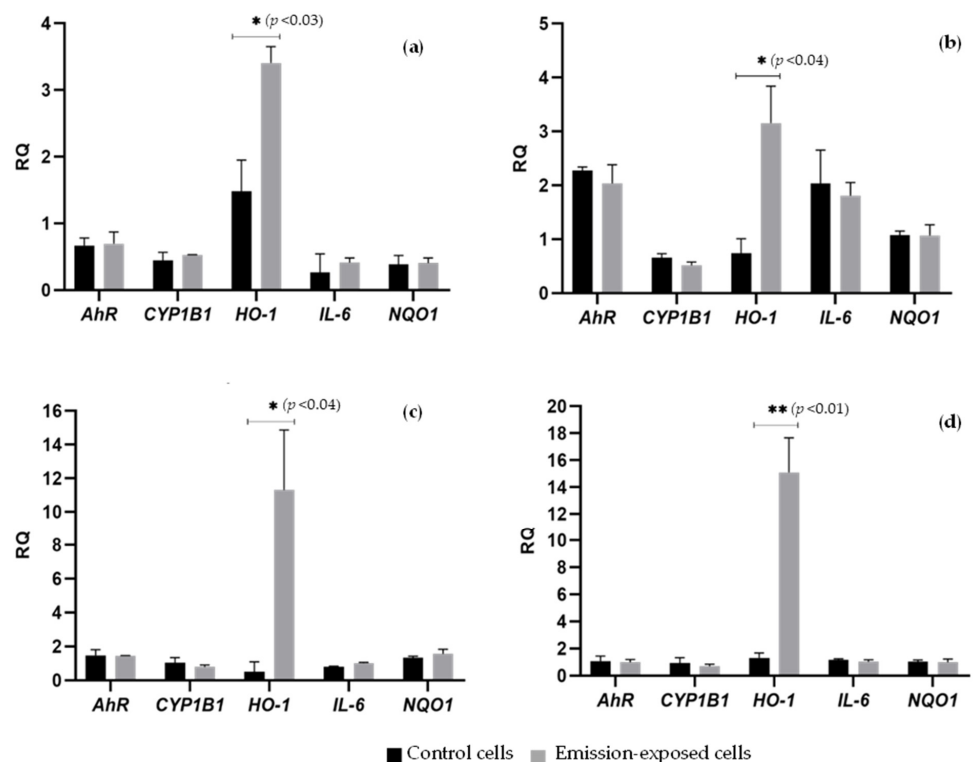


Figure A2. Gene expression of selected genes during the different biofuel blend emission tests. Biofuels I and III gene expression were analyzed just after the end of the tests (a,b), while for biofuels II and IV the cells were left to recover for 1 h after the end of the exposures (c,d). The recovery period dramatically increased the expression of the antioxidant HO1 gene. All the other genes were not modified.

References

1. Wu, Y.; Li, S.; Zhao, Q.; Wen, B.; Gasparrini, A.; Tong, S.; Overcenco, A.; Urban, A.; Schneider, A.; Entezari, A.; et al. Global, regional, and national burden of mortality associated with short-term temperature variability from 2000–2019: A three-stage modelling study. *Lancet Planet. Health* **2022**, *6*, e410–e421. [CrossRef]
2. Bellard, C.; Bertelsmeier, C.; Leadley, P.; Thuiller, W.; Courchamp, F. Impacts of climate change on the future of biodiversity. *Ecol. Lett.* **2012**, *15*, 365–377. [CrossRef] [PubMed]
3. Rinawati, F.; Stein, K.; Lindner, A. Climate Change Impacts on Biodiversity—The Setting of a Lingering Global Crisis. *Diversity* **2013**, *5*, 114–123. [CrossRef]
4. Heller, N.E.; Zavaleta, E.S. Biodiversity management in the face of climate change: A review of 22 years of recommendations. *Biol. Conserv.* **2009**, *142*, 14–32. [CrossRef]
5. Unfccc. Adoption of the Paris Agreement—Paris Agreement. In Proceedings of the Paris Climate Change Conference, Paris, France, 12 December 2015–22 April 2016.
6. European Commission. *Proposal Amending Regulations (EU) 2018/841 as Regards the Scope, Simplifying the Compliance Rules, Setting out the Targets of the Member States for 2030 and Committing to the Collective Achievement of Climate Neutrality by 2035 in the Land Use, Forestry and Agriculture Sector, and (EU) 2018/1999 as Regards Improvement in Monitoring, REPORTING, Tracking of Progress and Review*; European Commission: Brussels, Belgium, 14 July 2021. Available online: <https://eur-lex.europa.eu/legal-content/EN/TXT/?uri=CELEX%3A52021PC0554> (accessed on 15 September 2022).
7. European Commission. *Proposal Amending Regulation (EU) 2018/842 on Binding Annual Greenhouse Gas Emission Reductions by Member States from 2021 to 2030 Contributing to Climate Action to Meet Commitments under the Paris Agreement*; European Commission: Brussels, Belgium, 14 July 2021. Available online: <https://eur-lex.europa.eu/legal-content/EN/TXT/?uri=COM%3A2021%3A555%3AFIN> (accessed on 15 September 2022).
8. European Commission. *Proposal for a Regulation of the European Parliament and of the Council on Ensuring a Level Playing Field for Sustainable Air Transport*; European Commission: Brussels, Belgium, 2021; Available online: https://ec.europa.eu/transport/themes/mobilitystrategy_en (accessed on 3 August 2022).
9. Dedoussi, I.C. Implications of future atmospheric composition in decision-making for sustainable aviation. *Environ. Res. Lett.* **2021**, *16*, 031002. [CrossRef]
10. Debyser, A. ICAO Agreement on CO₂ Emissions from Aviation. Available online: <http://www.europarl.europa.eu/thinktank> (accessed on 3 August 2022).
11. Brasseur, G.P.; Gupta, M.; Anderson, B.E.; Balasubramanian, S.; Barrett, S.R.H.; Duda, D.P.; Fleming, G.G.; Forster, P.; Fuglestedt, J.S.; Gettelman, A.; et al. Impact of Aviation on Climate: FAA’s Aviation Climate Change Research Initiative (ACCRI) Phase II. *Bull. Am. Meteorol. Soc.* **2016**, *97*, 561–583. [CrossRef]
12. Gettelman, A.; Chen, C. The climate impact of aviation aerosols. *Geophys. Res. Lett.* **2013**, *40*, 2785–2789. [CrossRef]
13. Harrison, R.M.; Masiol, M.; Vardoulakis, S. Civil aviation, air pollution and human health. *Environ. Res. Lett.* **2015**, *10*, 041001. [CrossRef]
14. Kousoulidou, M.; Lonza, L. Biofuels in aviation: Fuel demand and CO₂ emissions evolution in Europe toward. *Transp. Res. Part D Transp. Environ.* **2016**, *46*, 166–181. [CrossRef]
15. Yilmaz, N.; Atmanli, A. Sustainable alternative fuels in aviation. *Energy* **2017**, *140*, 1378–1386. [CrossRef]
16. Prussi, M.; O’Connell, A.; Lonza, L. Analysis of current aviation biofuel technical production potential in EU28. *Biomass Bioenergy* **2019**, *130*, 105371. [CrossRef]
17. O’Connell, A.; Kousoulidou, M.; Lonza, L.; Weindorf, W. Considerations on GHG emissions and energy balances of promising aviation biofuel pathways. *Renew. Sustain. Energy Rev.* **2019**, *101*, 504–515. [CrossRef]
18. Lobo, P.; Hagen, D.E.; Whitefield, P.D. Comparison of PM Emissions from a Commercial Jet Engine Burning Conventional, Biomass, and Fischer–Tropsch Fuels. *Environ. Sci. Technol.* **2011**, *45*, 10744–10749. [CrossRef] [PubMed]
19. Anderson, A.; Karthikeyan, A.; Ramesh Kumar, C.; Ramachandran, S.; Praveenkumar, T.R. Lowest emission sustainable aviation biofuels as the potential replacement for the Jet-A fuels. *Aircr. Eng. Aerosp. Technol.* **2020**, *93*, 502–507. [CrossRef]
20. Moore, R.H.; Shook, M.; Beyersdorf, A.; Corr, C.; Herndon, S.; Knighton, W.B.; Miake-Lye, R.; Thornhill, K.L.; Winstead, E.L.; Yu, Z.; et al. Influence of Jet Fuel Composition on Aircraft Engine Emissions: A Synthesis of Aerosol Emissions Data from the NASA APEX, AAFEX, and ACCESS Missions. *Energy Fuels* **2015**, *29*, 2591–2600. [CrossRef]
21. E. European Union Aviation Safety Agency; E. European Environment Agency. *European Aviation Environmental Report Executive Summary and Recommendations*. 21 September 2022. pp. 1–24. Available online: <https://www.eea.europa.eu/highlights/european-aviation-environmental-report-2022> (accessed on 13 October 2022).
22. I. International Agency for Research on Cancer; IARC Working Group on the Evaluation of Carcinogenic Risks to Humans. Diesel And Gasoline Engine Exhausts and Some Nitroarenes Volume 105 Iarc Monographs on the Evaluation of Carcinogenic Risks to Humans. Available online: <https://monographs.iarc.who.int/wp-content/uploads/2018/06/mono105.pdf> (accessed on 13 October 2022).
23. Rahim, M.F.; Pal, D.; Ariya, P.A. Physicochemical studies of aerosols at Montreal Trudeau Airport: The importance of airborne nanoparticles containing metal contaminants. *Environ. Pollut.* **2018**, *246*, 734–744. [CrossRef]
24. Lopes, M.; Russo, A.; Monjardino, J.; Gouveia, C.; Ferreira, F. Monitoring of ultrafine particles in the surrounding urban area of a civilian airport. *Atmos. Pollut. Res.* **2019**, *10*, 1454–1463. [CrossRef]

25. Pirhadi, M.; Mousavi, A.; Sowlat, M.H.; Janssen, N.A.; Cassee, F.R.; Sioutas, C. Relative contributions of a major international airport activities and other urban sources to the particle number concentrations (PNCs) at a nearby monitoring site. *Environ. Pollut.* **2020**, *260*, 114027. [[CrossRef](#)]
26. Buonanno, G.; Bernabei, M.; Avino, P.; Stabile, L. Occupational exposure to airborne particles and other pollutants in an aviation base. *Environ. Pollut.* **2012**, *170*, 78–87. [[CrossRef](#)]
27. Marcias, G.; Casula, M.F.; Uras, M.; Falqui, A.; Miozzi, E.; Sogne, E.; Pili, S.; Pilia, I.; Fabbri, D.; Meloni, F.; et al. Occupational Fine/Ultrafine Particles and Noise Exposure in Aircraft Personnel Operating in Airport Taxiway. *Environments* **2019**, *6*, 35. [[CrossRef](#)]
28. Senkayi, S.N.; Sattler, M.L.; Rowe, N.; Chen, V.C. Investigation of an association between childhood leukemia incidences and airports in Texas. *Atmos. Pollut. Res.* **2014**, *5*, 189–195. [[CrossRef](#)]
29. Lin, S.; Munsie, J.P.; Herdt-Losavio, M.; Hwang, S.A.; Civerolo, K.; McGarry, K.; Gentile, T. Residential proximity to large airports and potential health impacts in New York State. *Int. Arch. Occup. Environ. Health* **2008**, *81*, 797–804. [[CrossRef](#)] [[PubMed](#)]
30. Harris, D.T.; Sakiestewa, D.; Titone, D.; Robledo, R.F.; Young, R.S.; Witten, M. Jet fuel-induced immunotoxicity. *Toxicol. Ind. Health* **2000**, *16*, 261–265. [[CrossRef](#)] [[PubMed](#)]
31. Jonsdottir, H.R.; Delaval, M.; Leni, Z.; Keller, A.; Brem, B.T.; Siegerist, F.; Schönenberger, D.; Durdina, L.; Elser, M.; Burtscher, H.; et al. Non-volatile particle emissions from aircraft turbine engines at ground-idle induce oxidative stress in bronchial cells. *Commun. Biol.* **2019**, *2*, 90. [[CrossRef](#)]
32. He, R.-W.; Gerlofs-Nijland, M.E.; Boere, J.; Fokkens, P.; Leseman, D.; Janssen, N.A.; Cassee, F.R. Comparative toxicity of ultrafine particles around a major airport in human bronchial epithelial (Calu-3) cell model at the air–liquid interface. *Toxicol.* **2020**, *68*, 104950. [[CrossRef](#)]
33. Stracquadiano, M.; Petralia, E.; Berico, M.; La Torretta, T.M.; Malaguti, A.; Mircea, M.; Gualtieri, M.; Ciancarella, L. Source Apportionment and Macro Tracer: Integration of Independent Methods for Quantification of Woody Biomass Burning Contribution to PM10. *Aerosol. Air Qual. Res.* **2019**, *19*, 711–723. [[CrossRef](#)]
34. Cheng, Y.; He, K.B.; Duan, F.K.; Zheng, M.; Ma, Y.L.; Tan, J.H. Positive sampling artifact of carbonaceous aerosols and its influence on the thermal-optical split of OC/EC. *Atmos. Chem. Phys.* **2009**, *9*, 7243–7256. [[CrossRef](#)]
35. Hwang, I.; Na, K. Filter- and Denuder-Based Organic Carbon Correction for Positive Sampling Artifacts. *Asian J. Atmos. Environ.* **2017**, *11*, 107–113. [[CrossRef](#)]
36. Herndon, S.C.; Shorter, J.H.; Zahniser, M.S.; Nelson, D.D.; Jayne, J.; Brown, R.C.; Miake-Lye, R.C.; Waitz, I.; Silva, P.; Lanni, T.; et al. NO and NO₂ Emission Ratios Measured from In-Use Commercial Aircraft during Taxi and Takeoff. *Environ. Sci. Technol.* **2004**, *38*, 6078–6084. [[CrossRef](#)]
37. Brown, R.C.; Miake-Lye, R.C.; Anderson, M.R.; Kolb, C.E.; Resch, T.J. Aerosol dynamics in near-field aircraft plumes. *J. Geophys. Res. Earth Surf.* **1996**, *101*, 22939–22953. [[CrossRef](#)]
38. Moore, R.; Thornhill, K.L.; Weinzierl, B.; Sauer, D.; D’Ascoli, E.; Kim, J.; Lichtenstern, M.; Scheibe, M.; Beaton, B.; Beyersdorf, A.J.; et al. Biofuel blending reduces particle emissions from aircraft engines at cruise conditions. *Nature* **2017**, *543*, 411–415. [[CrossRef](#)] [[PubMed](#)]
39. Gualtieri, M.; Grollino, M.G.; Consales, C.; Costabile, F.; Manigrasso, M.; Avino, P.; Aufderheide, M.; Cordelli, E.; Di Liberto, L.; Petralia, E.; et al. Is it the time to study air pollution effects under environmental conditions? A case study to support the shift of in vitro toxicology from the bench to the field. *Chemosphere* **2018**, *207*, 552–564. [[CrossRef](#)] [[PubMed](#)]
40. Lin, P.; Hu, S.-W.; Chang, T.-H. Correlation between gene expression of aryl hydrocarbon receptor (AhR), hydrocarbon receptor nuclear translocator (Arnt), cytochromes P4501A1 (CYP1A1) and 1B1 (CYP1B1), and inducibility of CYP1A1 and CYP1B1 in human lymphocytes. *Toxicol. Sci.* **2003**, *71*, 20–26. [[CrossRef](#)] [[PubMed](#)]
41. Kim, H.J.; Zheng, M.; Kim, S.-K.; Cho, J.J.; Shin, C.H.; Joe, Y.; Chung, H.T. CO/HO-1 Induces NQO-1 Expression via Nrf2 Activation. *Immune Netw.* **2011**, *11*, 376–382. [[CrossRef](#)] [[PubMed](#)]
42. Lee, S.E.; Jeong, S.I.; Yang, H.; Park, C.-S.; Jin, Y.-H.; Park, Y.S. Fisetin induces Nrf2-mediated HO-1 expression through PKC- δ and p38 in human umbilical vein endothelial cells. *J. Cell. Biochem.* **2011**, *112*, 2352–2360. [[CrossRef](#)]
43. Gao, J.; Zhao, S.; Halstensen, T.S. Increased interleukin-6 expression is associated with poor prognosis and acquired cisplatin resistance in head and neck squamous cell carcinoma. *Oncol. Rep.* **2016**, *35*, 3265–3274. [[CrossRef](#)]
44. Durdina, L.; Brem, B.; Abegglen, M.; Lobo, P.; Rindlisbacher, T.; Thomson, K.; Smallwood, G.; Hagen, D.; Sierau, B.; Wang, J. Determination of PM mass emissions from an aircraft turbine engine using particle effective density. *Atmos. Environ.* **2014**, *99*, 500–507. [[CrossRef](#)]
45. Hofmann, W.; Winkler-Heil, R.; Balásházy, I. The Effect of Morphological Variability on Surface Deposition Densities of Inhaled Particles in Human Bronchial and Acinar Airways. *Inhal. Toxicol.* **2006**, *18*, 809–819. [[CrossRef](#)]
46. Hansen, J.; Kharecha, P.; Sato, M.; Masson-Delmotte, V.; Ackerman, F.; Beerling, D.J.; Hearty, P.J.; Hoegh-Guldberg, O.; Hsu, S.-L.; Parmesan, C.; et al. Assessing “Dangerous Climate Change”: Required Reduction of Carbon Emissions to Protect Young People, Future Generations and Nature. *PLoS ONE* **2013**, *8*, e81648. [[CrossRef](#)]
47. Sher, F.; Raore, D.; Klemeš, J.J.; Rafi-Ul-Shan, P.M.; Khouzou, M.; Marintseva, K.; Razmkhah, O. Unprecedented Impacts of Aviation Emissions on Global Environmental and Climate Change Scenario. *Curr. Pollut. Rep.* **2021**, *7*, 549–564. [[CrossRef](#)]
48. Dray, L.; Evans, A.; Reynolds, T.; Schäfer, A. Mitigation of Aviation Emissions of Carbon Dioxide. *Transp. Res. Rec. J. Transp. Res. Board* **2010**, *2177*, 17–26. [[CrossRef](#)]

49. Krammer, P.; Dray, L.; Köhler, M. Climate-neutrality versus carbon-neutrality for aviation biofuel policy. *Transp. Res. Part D Transp. Environ.* **2013**, *23*, 64–72. [[CrossRef](#)]
50. Staples, M.D.; Malina, R.; Suresh, P.; Hileman, J.I.; Barrett, S.R. Aviation CO₂ emissions reductions from the use of alternative jet fuels. *Energy Policy* **2018**, *114*, 342–354. [[CrossRef](#)]
51. Beyersdorf, A.; Timko, M.; Ziemba, L.; Bulzan, D.; Corporan, E.; Herndon, S.; Howard, R.; Miake-Lye, R.; Thornhill, K.; Winstead, E. Reductions in aircraft particulate emissions due to the use of Fischer–Tropsch fuels. *Atmos. Chem. Phys.* **2014**, *14*, 11–23. [[CrossRef](#)]
52. Brem, B.T.; Durdina, L.; Siegerist, F.; Beyerle, P.; Bruderer, K.; Rindlisbacher, T.; Rocci-Denis, S.; Andac, M.G.; Zelina, J.; Penanhoat, O.; et al. Effects of Fuel Aromatic Content on Nonvolatile Particulate Emissions of an In-Production Aircraft Gas Turbine. *Environ. Sci. Technol.* **2015**, *49*, 13149–13157. [[CrossRef](#)]
53. Corbin, J.C.; Schripp, T.; Anderson, B.E.; Smallwood, G.J.; LeClercq, P.; Crosbie, E.C.; Achterberg, S.; Whitefield, P.D.; Miake-Lye, R.C.; Yu, Z.; et al. Aircraft-engine particulate matter emissions from conventional and sustainable aviation fuel combustion: Comparison of measurement techniques for mass, number, and size. *Atmos. Meas. Tech.* **2022**, *15*, 3223–3242. [[CrossRef](#)]
54. Voigt, C.; Kleine, J.; Sauer, D.; Moore, R.H.; Bräuer, T.; Le Clercq, P.; Kaufmann, S.; Scheibe, M.; Jurkat-Witschas, T.; Aigner, M.; et al. Cleaner burning aviation fuels can reduce contrail cloudiness. *Commun. Earth Environ.* **2021**, *2*, 114. [[CrossRef](#)]
55. Corporan, E.; DeWitt, M.J.; Belovich, V.; Pawlik, R.; Lynch, A.C.; Gord, J.R.; Meyer, T.R. Emissions Characteristics of a Turbine Engine and Research Combustor Burning a Fischer–Tropsch Jet Fuel. *Energy Fuels* **2007**, *21*, 2615–2626. [[CrossRef](#)]
56. Herndon, S.C.; Jayne, J.T.; Lobo, P.; Onasch, T.B.; Fleming, G.; Hagen, D.E.; Kaufmann, S.; Scheibe, M.; Jurkat-Witschas, T.; Miake-Lye, R.C. Commercial Aircraft Engine Emissions Characterization of in-Use Aircraft at Hartsfield-Jackson Atlanta International Airport. *Environ. Sci. Technol.* **2008**, *42*, 1877–1883. [[CrossRef](#)]
57. Kapadia, Z.Z.; Spracklen, D.V.; Arnold, S.R.; Borman, D.J.; Mann, G.W.; Pringle, K.J.; Monks, S.A.; Reddington, C.L.; Benduhn, F.; Rap, A.; et al. Impacts of aviation fuel sulfur content on climate and human health. *Atmos. Chem. Phys.* **2016**, *16*, 10521–10541. [[CrossRef](#)]
58. Zhang, X.; Karl, M.; Zhang, L.; Wang, J. Influence of Aviation Emission on the Particle Number Concentration near Zurich Airport. *Environ. Sci. Technol.* **2020**, *54*, 14161–14171. [[CrossRef](#)] [[PubMed](#)]
59. Møller, K.L.; Thygesen, L.C.; Schipperijn, J.; Loft, S.; Bonde, J.P.; Mikkelsen, S.; Brauer, C. Occupational Exposure to Ultrafine Particles among Airport Employees—Combining Personal Monitoring and Global Positioning System. *PLoS ONE* **2014**, *9*, e106671. [[CrossRef](#)] [[PubMed](#)]
60. Michaelis, S.; Loraine, T.; Howard, C.V. Ultrafine particle levels measured on board short-haul commercial passenger jet aircraft. *Environ. Health* **2021**, *20*, 89. [[CrossRef](#)] [[PubMed](#)]
61. Ren, J.; Liu, J.; Cao, X.; Li, F.; Li, J. Ultrafine particles in the cabin of a waiting commercial airliner at Tianjin International Airport, China. *Indoor Built Environ.* **2017**, *27*, 1247–1258. [[CrossRef](#)]
62. Barrett, S.R.H.; Britter, R.E.; Waitz, I.A. Global Mortality Attributable to Aircraft Cruise Emissions. *Environ. Sci. Technol.* **2010**, *44*, 7736–7742. [[CrossRef](#)]
63. Cavallo, D.; Ursini, C.L.; Carelli, G.; Iavicoli, I.; Ciervo, A.; Perniconi, B.; Rondinone, B.M.; Gismondi, M.; Iavicoli, S. Occupational exposure in airport personnel: Characterization and evaluation of genotoxic and oxidative effects. *Toxicology* **2006**, *223*, 26–35. [[CrossRef](#)]
64. Eastham, S.D.; Barrett, S.R. Aviation-attributable ozone as a driver for changes in mortality related to air quality and skin cancer. *Atmos. Environ.* **2016**, *144*, 17–23. [[CrossRef](#)]
65. Grilli, A.; Bengalli, R.; Longhin, E.; Capasso, L.; Proverbio, M.C.; Forcato, M.; Bicciato, S.; Gualtieri, M.; Battaglia, C.; Camatini, M.; et al. Transcriptional profiling of human bronchial epithelial cell BEAS-2B exposed to diesel and biomass ultrafine particles. *BMC Genom.* **2018**, *19*, 302. [[CrossRef](#)]
66. Lawal, A.O.; Zhang, M.; Dittmar, M.; Lulla, A.; Araujo, J.A. Heme oxygenase-1 protects endothelial cells from the toxicity of air pollutant chemicals. *Toxicol. Appl. Pharmacol.* **2015**, *284*, 281–291. [[CrossRef](#)]
67. Bendtsen, K.M.; Brostrøm, A.; Koivisto, A.J.; Koponen, I.; Berthing, T.; Bertram, N.; Kling, K.I.; Dal Maso, M.; Kangasniemi, O.; Poikkimäki, M.; et al. Airport emission particles: Exposure characterization and toxicity following intratracheal instillation in mice. *Part. Fibre Toxicol.* **2019**, *16*, 23. [[CrossRef](#)]
68. Riley, K.; Cook, R.; Carr, E.; Manning, B. A systematic review of the impact of commercial aircraft activity on air quality near airports. *City Environ. Interact.* **2021**, *11*, 100066. [[CrossRef](#)] [[PubMed](#)]
69. Othman, M.; Latif, M.T.; Hamid, H.H.A.; Uning, R.; Khumsaeng, T.; Phairuang, W.; Daud, Z.; Idris, J.; Sofwan, N.M.; Lung, S.-C.C. Spatial-temporal variability and health impact of particulate matter during a 2019–2020 biomass burning event in Southeast Asia. *Sci. Rep.* **2022**, *12*, 7630. [[CrossRef](#)] [[PubMed](#)]